Green Chemical Technology

SCIEPublish

Article

The Lanthanum-Modified Zeolite for Efficient Removal of Glyphosate: Adsorption Behaviors and Mechanisms

Xiaomeng Zhou [1,†], Junfeng Li [1,†], Mengmeng Deng [1], Xiaodi Li [1,*], Jinming Yi [1], Siqi Li [1], Junxia Yu [1], Chunqiao Xiao [1], Yuefei Zhang [1], Ruan Chi [1,2], Bo Hu [3], Jie Cao [3] and Songlin Zheng [3]

[1] State Key Laboratory of Green and Efficient Development of Phosphorus Resources, Key Laboratory of Novel Biomass-Based Environmental and Energy Materials in Petroleum and Chemical Industry, Hubei Novel Reactor & Green Chemical Technology Key Laboratory, Key Laboratory for Green Chemical Process of Ministry of Education, School of Chemistry and Environmental Engineering, Wuhan Institute of Technology, Wuhan 430079, China; 22309010139@stu.wit.edu.cn (X.Z.); 2209060124@stu.wit.edu.cn (J.L.); 22409010129@stu.wit.edu.cn (M.D.); 2309060430@stu.wit.edu.cn (J.Y.); 2309030233@stu.wit.edu.cn (S.L.); junxiay@wit.edu.cn (J.Y.); chunqiao@wit.edu.cn (C.X.); yuefeiz@wit.edu.cn (Y.Z.); rac@wit.edu.cn (R.C.)

[2] Hubei Three Gorges Laboratory, Yichang 443007, China

[3] Hubei Taisheng Chemical Co., Ltd., Yichang 443711, China; hubo888@xinfagroup.com (B.H.); caojie@xinfagroup.com (J.C.); songlinzheng@xinfagroup.com (S.Z.)

* Corresponding author. E-mail: 21071701@wit.edu.cn or xiaodipen@163.com (X.L.); Tel./Fax: +86-02787194980 (X.L.)

† These authors contributed equally to this work.

Received: 8 April 2026; Revised: 14 May 2026; Accepted: 16 July 2026; Available online: 31 July 2026

ABSTRACT: Glyphosate is one of the most extensively used organophosphorus herbicides; however, its excessive application and environmental residues have severely threatened aquatic ecosystems and human health. In this study, a highly efficient lanthanum-modified zeolite (LMZ) adsorbent was synthesized via a hydrothermal method, and its adsorption behaviors and underlying mechanisms for glyphosate removal were systematically investigated. LMZ exhibited exceptional adsorption performance over a broad pH range of 3.0–7.0, achieving a maximum adsorption capacity of 217.39 mg/g. The adsorption process was well described by the Langmuir isotherm and pseudo-second-order kinetic models, indicating a monolayer chemisorption process. Notably, LMZ demonstrated remarkable adsorption selectivity and excellent regenerability, maintaining a high adsorption capacity even after five consecutive adsorption-desorption cycles. In practical application assessments with simulated wastewater, glyphosate removal efficiency exceeded 90% at an adsorbent dosage of 7.5 g/L. Furthermore, dynamic column experiments confirmed that LMZ could maintain effective continuous adsorption, highlighting its substantial application potential for treating glyphosate-contaminated wastewater. X-ray photoelectron spectroscopy (XPS) and Raman spectroscopic characterizations revealed that this outstanding adsorption capability is primarily driven by inner-sphere complexation induced by ligand exchange at the La-OH active sites.

Keywords: Lanthanum-modified zeolite; Glyphosate; Adsorption; Ligand exchange

1. Introduction

N-(phosphonomethyl)glycine (glyphosate) is a broad-spectrum, low-residue, non-selective, and highly effective organophosphorus herbicide [1]. Due to these advantages, it is used extensively worldwide. According to relevant statistics, global annual use of glyphosate has surged from 67 million kg in 1995 to 826 million kg in 2014. Between 2005 and 2014, a staggering 6.1 billion kilograms of glyphosate were used worldwide, and it is projected to reach 7.4 to 9.2 million tons by 2025 [2,3]. The extensive use of glyphosate results in residues remaining in plants, entering the soil system, and being washed into water systems through precipitation. Glyphosate exhibits persistence, stability, and high toxicity in the environment [4]. It can persist in plants for decades or even longer [5] and easily leaches from plant roots into the soil [6]. The half-life of glyphosate and its metabolites in soil can reach up to 958 days [7]. Moreover, glyphosate can cause endocrine disruption and even DNA damage [8,9]. Compared to other aquatic pollutants, glyphosate poses unique challenges due to its massive global consumption and distinct organophosphorus characteristics [10,11]. Therefore, the treatment of high-concentration organophosphorus pollutants is of significant environmental importance.

Currently, the main methods for treating glyphosate-containing wastewater include biological treatment, adsorption, and advanced oxidation processes [12–14]. However, advanced oxidation and biological treatment methods may produce AMPA, a byproduct that is even more toxic than glyphosate itself, during the treatment process [15]. In comparison to these two methods, adsorption has the advantages of simple design, non-toxicity, low cost, and high removal efficiency, making it widely used in practical applications. To date, a variety of adsorbents have been developed for glyphosate removal. Among the numerous metal-based phosphate adsorbents, lanthanum-based adsorbents have been extensively studied due to the strong affinity of lanthanum, good metal stability, and strong anti-interference ability [16]. Compared with conventional, cheaper transition metals such as iron or aluminum, lanthanum, acting as a hard Lewis acid, exhibits a significantly higher specific affinity for phosphate groups (hard Lewis bases). This specific inner-sphere complexation enables lanthanum-based materials to maintain superior adsorption capacities and high selectivity even in the presence of complex competing anions and over a broader pH range. For example, Wu et al. used a hydrothermal method to load lanthanum oxide onto diatomaceous earth, creating a highly efficient phosphate adsorbent. Through electrostatic interactions, ligand exchange, and Lewis acid-base interactions, the maximum phosphate adsorption capacity reached 58.7 mg P/g [17]. Similarly, Wei et al. prepared lanthanum-doped ordered mesoporous hollow silica spheres, achieving a maximum phosphate adsorption capacity of 47.89 mg P/g [18]. Jin et al. utilized lanthanum-modified copper tailings, thereby increasing their phosphate adsorption capacity from 0.73 mg/g to 7.07 mg/g [19]. Jia et al. developed a lanthanum-modified biochar adsorbent, which achieved a phosphate adsorption capacity of 124.61 mg P/g at 25 °C [20].

As a widely used class of adsorbents, zeolites have garnered significant attention in environmental remediation due to their well-defined porous structures, high specific surface areas, and exceptional ion-exchange capacities. While traditional zeolites synthesized from pure chemical reagents are highly effective, their substantial production costs often limit large-scale applications. Consequently, the synthesis of zeolites using various low-cost natural materials and industrial solid wastes as precursors has emerged as an economically and environmentally viable strategy. For example, Cyrille et al. synthesized zeolites using natural kaolin, which exhibited maximum adsorption capacities of 780, 600, 1000, and 1300 mg/g for Sr^{2+}, In^{3+}, Ni^{2+}, and Co^{2+}, respectively [21]. Sivamani synthesized mesoporous zeolite Y using rice husk ash as the raw material, achieving a maximum adsorption capacity of 3.38 mg/g for As(V) [22]. Chang et al. explored the optimum processing parameters for the synthesis of zeolite from coal gangue; the findings demonstrated that, under the optimal conditions, the maximum adsorption capacities toward Cd and Pb reached 181.3 and 419.9 mg/L, respectively [23].

In our previous research, an efficient adsorbent of lanthanum-modified zeolite was synthesized from fly ash using a hydrothermal method, and the material exhibited good phosphate adsorption performance while being resistant to interference from coexisting ions, pH, and aerobic/anaerobic environmental factors [24–26]. However, the adsorption performance and mechanism of this material with respect to organic phosphorus have not been thoroughly studied, which is crucial for its application in phosphorus-containing wastewater treatment.

In this study, the main objective is to explore the adsorption behaviors and mechanism of lanthanum-modified zeolite for glyphosate, and evaluate its potential for practical application. Batch adsorption experiments were conducted to determine the adsorption capacity and effects of pH and coexisting ions on glyphosate adsorbed by LMZ. Further, the adsorption performance of LMZ for glyphosate removal in simulated wastewater and under dynamic conditions was investigated. Finally, the adsorbent was characterized by SEM, FT-IR and XPS methods, to reveal the adsorption mechanism. Because of its simple preparation process, low cost, and large-scale utilization of coal fly ash, it is expected to become a highly efficient glyphosate adsorbent.

2. Materials and Methods

2.1. Materials

The lanthanum-modified zeolite (LMZ) used in the experiments was prepared following a method described by Xie et al. [25]. In brief, coal fly ash was first treated with a 2.0 M NaOH solution at 95 °C for 24 h, using a solid-to-liquid ratio of 150 g of fly ash to 900 mL of NaOH solution. After cooling the mixture to room temperature, 900 mL of a 2 M $LaCl_3$ solution was slowly added at a rate of 10 mL/min under continuous stirring. The resulting LMZ was thoroughly rinsed with ethanol and deionized water, dried, and sieved for use in the experiments. All chemicals, including glyphosate, sodium hydroxide, hydrochloric acid, lanthanum chloride, sodium chloride, sodium sulfate, sodium nitrate, and sodium bicarbonate, were of analytical grade.

2.2. Batch Adsorption Experiments

All batch adsorption experiments, including adsorption isotherm, kinetics, pH, adsorption dosage, and co-ions, were conducted in an oscillator (250 rpm) at room temperature. The concentrations of glyphosate were determined by the molybdenum-blue ascorbic acid method. For the adsorption isotherm experiments, 0.1 g of LMZ was dispersed into 40.00 mL glyphosate solution with initial concentrations ranging from 200 to 1000 mg/L. The adsorption kinetics experiments were performed after adding 0.1 g of LMZ to 40 mL of glyphosate with a concentration of 400 mg/L. The effects of pH on adsorption performance were evaluated in the range of 2–11, at a concentration of 400 mg/L. The dosage experiments were proceeded by adding 0.05–0.5 g into glyphosate solution with a concentration of 400 mg/L. It's worth noting that, to simulate the treatment effect of adsorbents in real wastewater, tap water was used to dispense the glyphosate solution in this experiment. The last co-ion tests were performed using a 400 mg/L glyphosate solution containing co-ions, including sodium sulfate, sodium nitrate, sodium chloride, and sodium bicarbonate. The molar ratio of coexisting ions to glyphosate is 1:25. A cyclic regeneration experiment was conducted at pH 7 to evaluate the reusability of LMZ. Specifically, 0.1 g of LMZ was added to 40 mL of glyphosate solution with an initial concentration of 400 mg/L. After reaching adsorption equilibrium, the adsorbent was collected and subjected to desorption in a 4 M NaOH solution. This adsorption–desorption cycle was repeated five times, and the adsorption capacity of LMZ was measured after each cycle.

2.3. Dynamic Adsorption Experiments

The dynamic adsorption experiments were conducted in a laboratory-scale fixed-bed column with an inner diameter of 1 cm and a height of 20 cm. Specifically, 1.0 g of LMZ was fixed in the column, and the glyphosate solution (the initial concentration was 300 mg/L) was pumped into the column by peristaltic pump at a fixed flow rate. Then the Breakthrough curves could be drawn by collecting samples at different times, and the adsorption amounts of the glyphosate at time *t* also could be calculated by the equations. To explore the effects of flow rate on Breakthrough curves, three different velocities of flow (2.5, 5.0 and 7.5 mL/min) were set in this experiment.

2.4. Characterization

To further analyze the adsorption mechanism of LMZ, a combination of characterization techniques was employed in this study. The surface morphology and elemental distribution were observed using a scanning electron microscope (SEM, Hitachi S4800, Tokyo, Japan). Fourier-transform infrared spectroscopy (FT-IR, Thermo Fisher, Waltham, MA, USA) was used to analyze changes in surface functional groups before and after adsorption. The Zeta potential was measured using a Zeta Sizer Nano-ZS90 (Malvern Instruments, Malvern, UK). In addition, X-ray photoelectron spectroscopy (XPS, Thermo Fisher, Waltham, MA, USA) was employed to characterize the changes in the surface chemical states of the material before and after adsorption.

3. Results and Discussion

3.1. Effect of Initial Concentration

As demonstrated in Figure 1a, the effect of glyphosate initial concentration on the adsorption performance of LMZ is illustrated, with the results indicating that as the initial glyphosate concentration increases, the adsorption capacity of LMZ rapidly increases until equilibrium is reached. With further increases in glyphosate concentration, the adsorption capacity stabilises, ultimately reaching approximately 200 mg/g. In comparison, studies by Zhao et al. [24]. and Xie et al. [25] showed that unmodified zeolites exhibited a maximum phosphate adsorption capacity of only 10 mg/g, while Siamak Zavareh reported a glyphosate adsorption capacity of only 30 mg/g using 4A zeolite [27]. Therefore, the excellent adsorption performance of LMZ for glyphosate may be attributed to the presence of abundant La active sites on the adsorbent surface. A similar phenomenon was observed by Jin et al., who, in developing $La(OH)_3$-modified copper tailings, found that the introduction of lanthanum resulted in a phosphorus adsorption capacity approximately 10 times higher than that of the original copper tailings [19]. Additionally, we have also plotted the corresponding thermodynamic curves. As depicted in Figure S1, the adsorption capacity of LMZ for glyphosate increases markedly with increasing temperature. This positive temperature dependence clearly indicates the endothermic nature of the interfacial adsorption process. In addition, we have surveyed the relevant literature and compared the adsorption performance of our material with other adsorbents. As shown in Table S4, LMZ possesses a superior adsorption capacity for glyphosate.

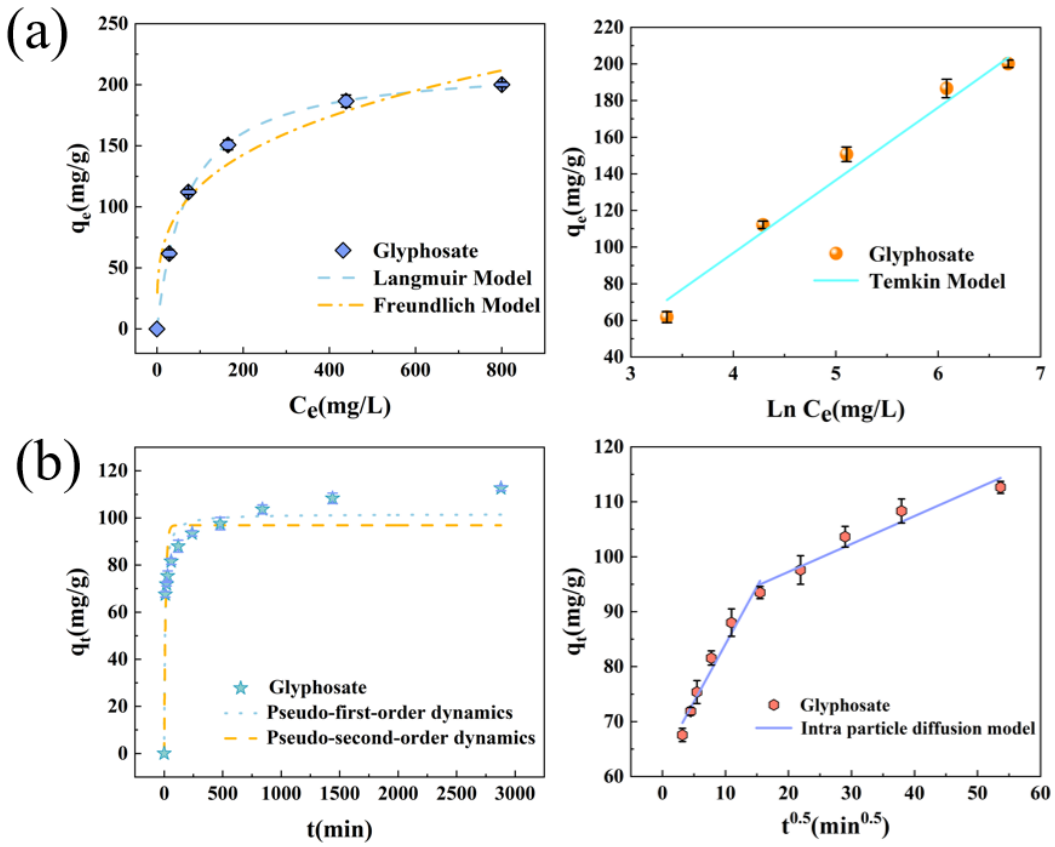

Figure 1. (**a**) Adsorption isotherms of glyphosate on LMZ, (**b**) Adsorption kinetics of glyphosate on LMZ.

In an attempt to further understand adsorption behavior, three adsorption isotherm models were used to fit the experimental data. The specific formulas and parameters of the three models are shown as follows:

Langmuir Model

$$q_e = \frac{q_m C_e}{1/b + C_e} \tag{1}$$

Freundlich Model

$$q_e = K_f C_e^{1/n} \tag{2}$$

Temkin Model

$$q_e = \frac{RT}{b_T} lnA_T + \frac{RT}{b_T} lnC_e = BlnA_T + BlnC_e \tag{3}$$

In the equation, q_e is the equilibrium adsorption capacity (mg/g), q_m is the maximum adsorption capacity (mg/g), and C_e is the equilibrium concentration of solute (mg/L). b represents the adsorption equilibrium constant (L/mg); K_f is the Freundlich affinity coefficient ((mg/g)/(mg/L)$^{1/n}$), and n is the Freundlich affinity coefficient. $B = RT/b_T$, b_T is the Temkin constant related to the heat of adsorption (J·mol^{-1}), A_T is the Temkin isotherm equilibrium binding constant (L·g^{-1}), R is the gas constant (8.3145 J·mol^{-1}·K^{-1}), and T is the absolute temperature at 298.15 K.

The fitting parameters of the three models are shown in Table S1. The R^2 values for the three models are 0.9997, 0.9703, and 0.9834, respectively, and their corresponding reduced chi-square (χ^2) values are 1.54, 219.79, and 72.21, respectively. The Langmuir model fitted the data best compared with the

Freundlich and Temkin models. This indicated that the adsorption process of LMZ on glyphosate was in accordance with the assumptions of Langmuir theory, *i.e.*, the surface of LMZ provided a finite number of active adsorption sites, and the adsorption process was a monomolecular layer adsorption. The Langmuir model was able to predict a maximum adsorption amount of 217.39 mg/g, which was in good agreement with the experimental data. Furthermore, the Freundlich model fitting results indicated that the 1/*n* value was less than 1, suggesting that the adsorption of glyphosate was spontaneous and implying favourable glyphosate adsorption on LMZ [28,29]. The Temkin model also demonstrated a high degree of goodness of fit, suggesting that the adsorption process involved physical adsorption, with a heat of adsorption of 62.44 J/mol.

3.2. Effect of Contact Time

As demonstrated in Figure 1b, the adsorption kinetics of LMZ on glyphosate were investigated by varying the contact time, and the adsorption process was evident to be categorised into two distinct phases. The initial 240 min constituted the rapid adsorption process, following which the adsorption rate underwent a gradual decline until achieving adsorption equilibrium. The rapid initial adsorption is primarily ascribed to the uniform dispersion of La on the surface of the fly ash-derived zeolite, which facilitates the availability of numerous active sites for glyphosate binding [30,31]. The rapid adsorption of glyphosate by LMZ indicates its considerable potential in practical wastewater treatment.

In order to further clarify the adsorption process, three kinetic models were used to fit the experimental data. The equations are shown below, where q_e is the equilibrium adsorption capacity (mg/g), k_1 is the rate constant of the first-order kinetic equation, k_2 is the rate constant of the second-order kinetic equation, k_p is the intraparticle diffusion rate constant, and C is a constant.

Pseudo-first-order model

$$q_t = q_e\left[1 - e^{(-k_1 t)}\right] \tag{4}$$

Pseudo-second-order model

$$\frac{t}{q_t} = \frac{1}{k_2 q_e^2} + \frac{t}{q_e} \tag{5}$$

Intra particle diffusion model

$$q_t = k_p t^{0.5} + C \tag{6}$$

As demonstrated in Table S2, the three models were found to have distinct specific fitting parameters. The pseudo-second-order kinetic model demonstrated the highest R^2 value of 0.949 and the lowest χ^2 value of 53.59, indicating that chemisorption is the predominant mode in the adsorption process. The q_{max} value obtained from this model was 110 mg/g, which was in close agreement with the 112 mg/g value obtained from the actual experiment. In the intraparticle diffusion model (Figure 1b), the adsorption of glyphosate onto LMZ exhibited a two-stage linear profile, indicating that the process involves both film diffusion and intraparticle diffusion mechanisms [32]. The intercept (C) was not equal to zero, suggesting that intraparticle diffusion was not the sole rate-limiting step; instead, both film diffusion and intraparticle diffusion jointly controlled the adsorption process [33,34]. The rate constants k_{p1} and k_{p2} were 2.09 and 0.51, respectively. The significantly higher k_{p1} value implies that the initial rapid adsorption was governed by film diffusion, whereas the subsequent decrease in adsorption rate was mainly limited by intraparticle diffusion [35]. Specifically, during the early stage, glyphosate was rapidly adsorbed onto the external surface of LMZ via film diffusion. Once the surface active sites became saturated, glyphosate molecules gradually penetrated into the interior of the particles and were adsorbed onto internal sites. As the internal

concentration of glyphosate increased, diffusion resistance also increased, leading to a further reduction in the intraparticle diffusion rate [36]. These data provide valuable guidance for determining the hydraulic retention time (HRT) in practical engineering applications. Since the length of the HRT directly determines the utilization efficiency of the adsorbent, it is essential to optimize the HRT to adequately accommodate the intra-particle diffusion stage.

3.3. pH Effect on Glyphosate Adsorption

As demonstrated in Figure 2a, the pH of the solution has a direct impact on the adsorption of glyphosate by LMZ. This clearly demonstrates that the adsorption of glyphosate by LMZ is closely related to the pH of the system. At a pH range of 3–7, glyphosate adsorption exhibited minimal variation. However, under alkaline conditions, the amount adsorbed decreased dramatically, and a similar phenomenon was observed in the studies by Wang et al. [37] and Yang et al. [38]. The extremely low adsorption of glyphosate at a pH of 2 was due to the dissolution of La in LMZ, as proved in preliminary LMZ leaching experiments [25].

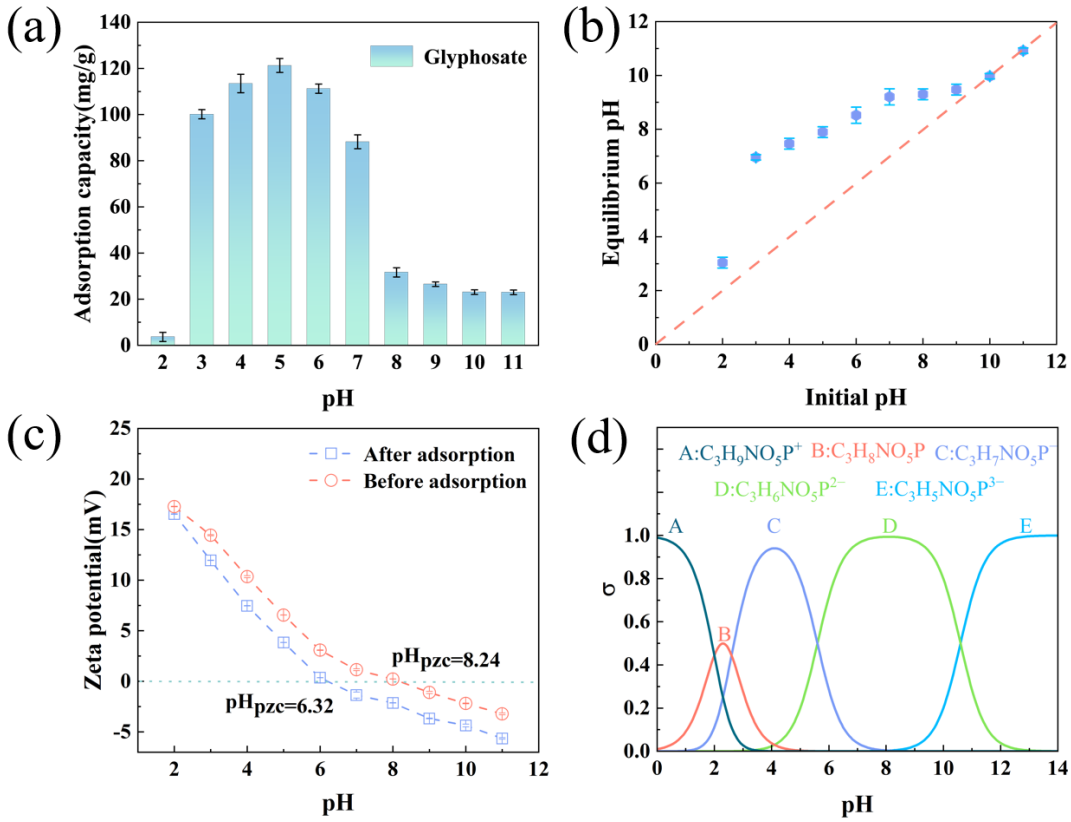

Figure 2. (**a**) pH effect on glyphosate adsorption, (**b**) The change in pH of the system before and after adsorption, (**c**) The zeta potential of LMZ before and after glyphosate adsorption, (**d**) The distribution of glyphosate species at different pH levels.

To further elucidate the adsorption mechanism, the point of zero charge (pH_{pzc}) of LMZ was measured before and after glyphosate adsorption, and the equilibrium pH of the solution was recorded. In addition, the speciation of glyphosate at different pH levels was calculated. As shown in Figure 2c, the pH_{pzc} of LMZ decreased from 8.24 before adsorption to 6.32 after adsorption, consistent with findings reported by Kovács et al. [39] and Waiman et al. [40]. Figure 2d illustrates the distribution of the five dominant protonation states of glyphosate over a range of pH values. When the solution pH is below the pH_{pzc}, the surface of LMZ becomes positively charged due to protonation, forming La-OH_2^+ species [30], while glyphosate mainly exists as $C_3H_7NO_5P^-$ and $C_3H_6NO_5P^{2-}$. These anionic species can be effectively adsorbed via electrostatic attraction and ligand exchange. The observed increase in solution pH after adsorption (Figure

2b) further confirms that glyphosate interacts with protonated La-OH^{2+} groups, thereby releasing hydroxide ions via ligand exchange. In contrast, when the pH exceeds the pH_{pzc}, the surface of LMZ becomes negatively charged, resulting in electrostatic repulsion that hinders glyphosate adsorption. Additionally, excess hydroxide ions in alkaline conditions compete with glyphosate for active sites, suppressing ligand exchange. This interpretation is supported by the relatively stable pH observed under alkaline conditions. At very low pH (e.g., pH 2), lanthanum hydroxide species may dissolve, but the porous structure and capillary channels of the zeolite matrix still enable a limited amount of glyphosate to be retained via physical adsorption [41]. Overall, the primary mechanisms governing glyphosate removal by LMZ are ligand exchange and electrostatic interaction, while physical adsorption plays a secondary role.

3.4. Effect of Dosage on Glyphosate Removal

The effects of sorbent dosage on glyphosate removal were shown in Figure 3a. At dosages of 1.25, 2.5, 5, 7.5, 10, and 12.5 g/L, the removal efficiency of glyphosate increased from 35% to 53%, 84%, 95%, 96%, and 97%, respectively. In the initial stage, the amount of adsorbent was insufficient to capture all the phosphorus, but as the dosage increased, the removal efficiency gradually improved. This can be attributed to the increased availability of surface area and active center sites, which enhanced glyphosate adsorption. However, an excessive dosage may lead to material wastage. From the perspective of cost control and removal efficiency, the optimal adsorbent dosage was 7.5 g/L for treating 400 mg/L glyphosate wastewater.

3.5. Effect of Co-Ions on Glyphosate Adsorption and the Reusability of LMZ

In real wastewater, a variety of coexisting anions and cations—such as Cl^-, NO_3^-, SO_4^{2-} and HCO_3^-—may influence glyphosate adsorption by competing for active sites on the adsorbent surface. As shown in Figure 3b, Cl^- and NO_3^- exerted negligible effects on the adsorption performance of LMZ, whereas SO_4^{2-} reduced the adsorption capacity by approximately 10%. This effect is likely attributed to the divalent nature of SO_4^{2-}, which enhances Coulombic repulsion and interferes with the interaction between glyphosate and active adsorption sites [42]. Notably, the sulfate concentration used in this test was 6620 mg/L—25 times higher than that of glyphosate—whereas actual sulfate levels in wastewater are generally much lower, suggesting that such interference would be minimal under practical conditions. In contrast, the presence of HCO_3^- had a pronounced inhibitory effect, reducing the adsorption capacity to approximately 20 mg/g. This suppression can be attributed to two primary factors: first, the addition of HCO_3^- increased the solution pH to ~8.0, a condition under which the adsorption of glyphosate had already declined to 31 mg/g (as shown in Figure 2a); and second, the formation of CO_3^{2-} in the solution may compete with glyphosate for La binding sites, potentially forming $La_2(CO_3)_3$ [43], thereby occupying active sites and inhibiting the complexation between La and glyphosate. These observations further support the conclusion that inner-sphere complexation is the dominant mechanism of glyphosate adsorption onto LMZ, which also explains its relatively high tolerance to the presence of most common anions. The reusability of LMZ was evaluated over five consecutive adsorption–desorption cycles. As shown in Figure 3c, the adsorption capacity decreased from 83.58 mg/g to 67.76 mg/g. This reduction could be attributed to minor material loss during handling, as well as the incomplete desorption of glyphosate, which may have resulted in the occupation of active sites in subsequent cycles. As shown in Figure 3d, the desorption efficiency gradually declined from 97% to 85% with increasing cycle number, indicating that a portion of glyphosate was strongly bound to LMZ and was difficult to desorb. Nevertheless, these results demonstrate that LMZ exhibits excellent regeneration performance and holds strong potential for practical application in the treatment of glyphosate-contaminated wastewater.

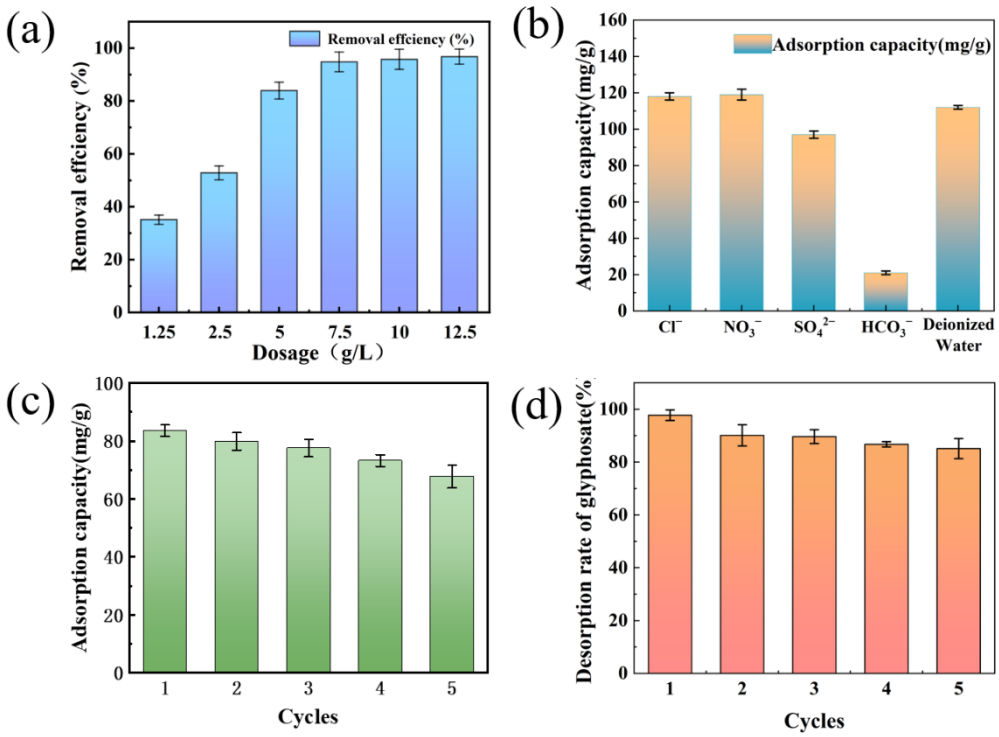

Figure 3. (**a**) Effect of adsorbent dosage on removal efficiency, (**b**) Influence of coexisting ions on glyphosate adsorption, (**c**) Adsorption capacity of LMZ in five adsorption–desorption cycles, (**d**) Desorption performance of LMZ in five adsorption–desorption cycles.

3.6. Adsorption Mechanism

3.6.1. XRD and XRF Analysis

Figure S2 displays the X-ray diffraction (XRD) patterns of the pristine zeolite and LMZ. The synthesized material exhibits the distinct characteristic diffraction peaks of zeolite, confirming its successful synthesis. Notably, no prominent new peaks emerge in the pattern of LMZ, indicating that the loaded La species exist in an amorphous state on the zeolite. Table S3 presents the XRF chemical composition analysis of LMZ, indicating that the primary components are SiO_2 and La_2O_3, with La_2O_3 accounting for 34.7%.

3.6.2. Mapping Analysis

The SEM image of LMZ (Figure 4a) reveals uniformly distributed spherical nanoparticles on the surface of the synthesized material, with particle sizes within the nanoscale range. The incorporation of La also leads to the formation of numerous pores on the zeolite surface, increasing the material's specific surface area and exposing more active adsorption sites, thereby enhancing its capacity to adsorb target pollutants. Following glyphosate adsorption, the SEM image of LMZ (Figure 4b) shows that the spherical particles on the surface are larger and more densely packed than in the unadsorbed sample. This morphological change is attributed to the successful adsorption of glyphosate onto LMZ. A similar phenomenon was also observed in the study conducted by Sufia et al. [44]. This morphological change on the surface of LMZ indicates its capability to separate glyphosate from aqueous solutions.

Figure 4c shows the elemental distribution maps after glyphosate adsorption by LMZ. It can be seen that the distribution of Si, Al, O, and Na are relatively similar, because that the synthesized zeolite is a kind of silico-aluminate mineral. In addition, the element of La is evenly distributed on the surface of zeolite, indicating that La introduced in the synthesis process is well loaded on the surface of zeolite. And the

distribution of P almost overlapped with that of La after adsorption, which indicates that lanthanum oxide on the surface of zeolite is the main adsorption site for glyphosate.

3.6.3. FTIR Analysis

Figure 4b presents the FTIR spectra of LMZ before and after glyphosate adsorption. For the original LMZ, a prominent peak is observed at approximately 3209 cm^{-1}, which corresponds to the O–H stretching vibration on the surface of LMZ. After glyphosate adsorption, the intensity of this peak decreases, which may be attributed to the exchange of O–H with glyphosate and the formation of inner-sphere complexes [45]. Additionally, the broadening of this peak after adsorption suggests the introduction of N–H groups from glyphosate. The peak at 984 cm^{-1} shows no significant change before and after adsorption, likely due to the inherent Si–O structure of the material. A new peak appears at 1079 cm^{-1} in the LMZ spectrum after adsorption, which can be attributed to the vibrations of the phosphate groups in glyphosate. Moreover, another new peak emerges at 1330 cm^{-1}, corresponding to the carboxyl functional groups of glyphosate [4,46], further confirming the successful adsorption of glyphosate onto LMZ.

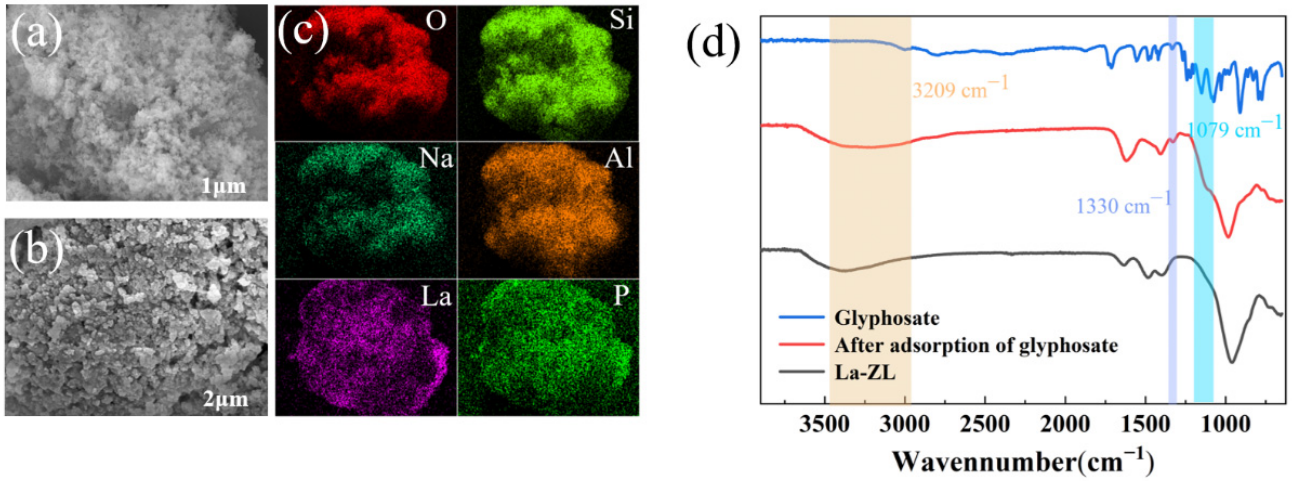

Figure 4. (**a**) SEM image of LMZ, (**b**) SEM image of LMZ after glyphosate adsorption, (**c**) the elemental distribution maps after glyphosate adsorption by LMZ, (**d**) the FTIR spectra of LMZ before and after glyphosate adsorption.

3.6.4. XPS Analysis

Through XPS analysis, we can further understand the adsorption mechanism of LMZ for glyphosate. The full spectrum of LMZ before and after glyphosate adsorption is shown in Figure 5a. It can be observed that after adsorption, a distinct P 2p orbital peak appears at approximately 133.08 eV, and an N 1s peak emerges at 400.26 eV. Both of these findings demonstrate that glyphosate was adsorbed onto LMZ through interaction [47,48].

Figure 5b shows the spectra of La 3d5/2 before and after glyphosate adsorption. The representative characteristic peaks of the original La 3d5/2 are centered on 834.92 eV and 838.45 eV, respectively. After adsorption, both characteristic peaks of La shift toward higher binding energies, appearing at 835.18 eV and 838.61 eV, respectively. The phenomenon that the double characteristic peaks shift toward the direction of high binding energy is often observed in the process of La-based hydrates (oxides) adsorbing phosphate, which is interpreted as the result of electron transfer from the valence band of the ligand atom to the 4f orbital of the La atom [30,35,49]. The large shifts of 0.26 eV and 0.16 eV suggest strong affinities on the metal oxide surface, likely due to the formation of potential monodentate and bidentate inner-sphere surface complexes.

The O 1s energy spectrum before and after adsorption are shown in Figure 5c. According to the binding energy of different oxygen, the O 1s spectrum can be divided into three characteristic peaks corresponding

to M–O at 530.24 eV (bonding of oxygen to metal), M–OH at 531.48 eV (bonding of hydroxyl group to metal), and adsorbed water at 532.34 eV (H_2O). After glyphosate adsorption, the relative area of the La–O peak increased from 26.44% to 46.43%, while that of the La–OH peak decreased from 62.00% to 29.06%, which confirmed that glyphosate was adsorbed through ligand exchange with hydroxyl groups on the surface of the material. In the pH influence experiment, it was also observed that the system's pH increased significantly after the reaction, indicating that the hydroxyl group was replaced and that a complex formed between glyphosate and the lanthanum adsorption site. Figure 5d shows the high-resolution spectrum of P, where a distinct P 2p peak is observed after adsorption, with a binding energy located at 132.66 eV. This indicates the formation of metal phosphate compounds, confirming the complexation between La and glyphosate [35]. Interestingly, the P 2p spectrum can be well-fitted with a single component, a similar phenomenon observed in the study by G. Ruano et al. [47].

3.6.5. Roman Analysis

Figure 6a displays the Raman spectra of LMZ before and after glyphosate adsorption. Prior to adsorption, pristine LMZ exhibits distinct characteristic peaks at wavenumbers of 147, 437, and 615 cm^{-1}, which are assigned to the typical vibrational modes of $La(OH)_3$. This observation is highly consistent with the findings reported by Atsuya et al., who demonstrated that the standard Raman spectrum of $La(OH)_3$ displays peaks at 140, 227, 283, 342, 450, and 603 cm^{-1}. However, following glyphosate adsorption, the intensities of these three characteristic peaks are significantly attenuated. This indicates that when glyphosate molecules replace the surface hydroxyl groups of LMZ to form inner-sphere complexes, the original localized lattice symmetry of the La–OH bonds is disrupted, thereby leading to the broadening and quenching of the characteristic Raman peaks. Furthermore, a new peak emerges at 990 cm^{-1} in the spectrum after adsorption. This new peak is attributed to the stretching vibration of the P–O–X band (where X denotes a hydrogen or metal atom bonded to the phosphate group), which further verifies the formation of inner-sphere complexes. Collectively, these spectroscopic phenomena provide compelling evidence that LMZ and glyphosate form stable inner-sphere complexes primarily through a ligand exchange mechanism.

Based on the preceding analyses, the adsorption mechanism of glyphosate onto LMZ is primarily governed by chemisorption via ligand exchange, with electrostatic attraction serving as an auxiliary pathway. The excellent fit of the pseudo-second-order kinetic model, combined with the XPS results, corroborates that ligand exchange and inner-sphere complexation are the predominant driving forces in the adsorption process. Specifically, the active $La(OH)_3$ sites on the LMZ surface undergo ligand exchange with glyphosate molecules, subsequently releasing OH^- ions into the solution. Consequently, LMZ can retain a substantial adsorption capacity for glyphosate even under alkaline conditions. Meanwhile, owing to the inherent porous structure of the zeolite matrix, its surface macropores and internal capillary channels can capture a minor fraction of glyphosate through physisorption (Figure 6b). When the solution pH is below the point of zero charge (pH_{pzc}), the protonated hydroxyl groups on the adsorbent surface further promote glyphosate adsorption via electrostatic attraction. Ultimately, this synergistic multiple-mechanism pathway empowers LMZ to effectively sequester glyphosate despite pH fluctuations and the presence of interfering anions.

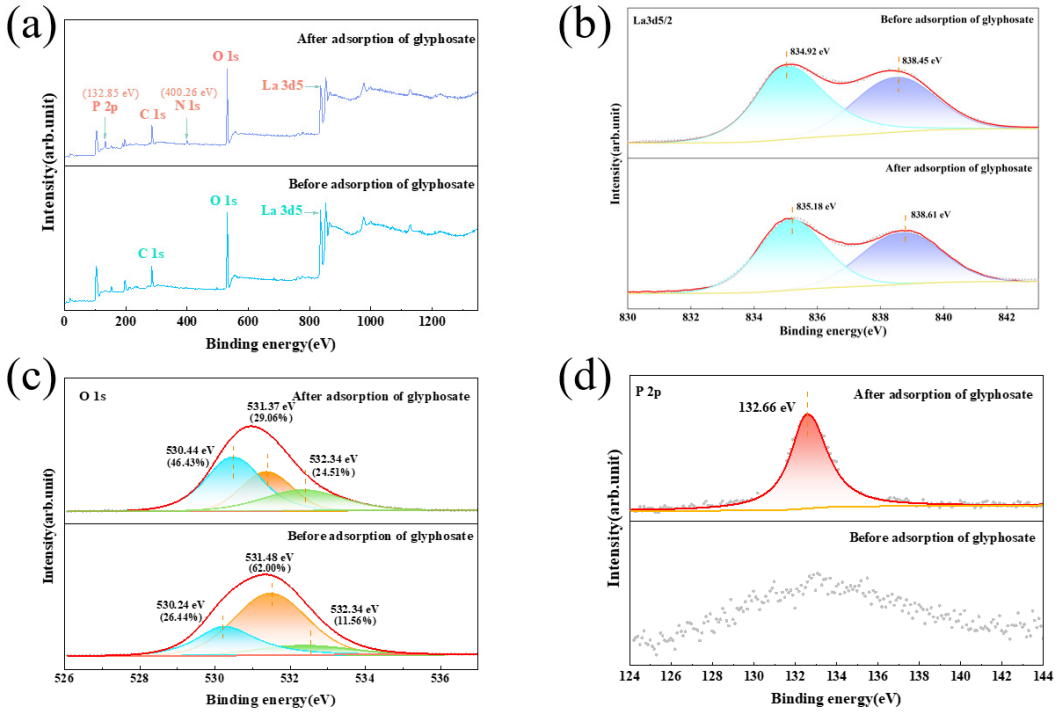

Figure 5. XPS analysis of LMZ before or after glyphosate adsorption. (**a**) XPS survey scan of LMZ before and after glyphosate adsorption, (**b**) La 3d5/2 spectra before and after glyphosate adsorption, (**c**) O 1s spectra before and after glyphosate adsorption, (**d**) P 2p spectra before and after glyphosate adsorption.

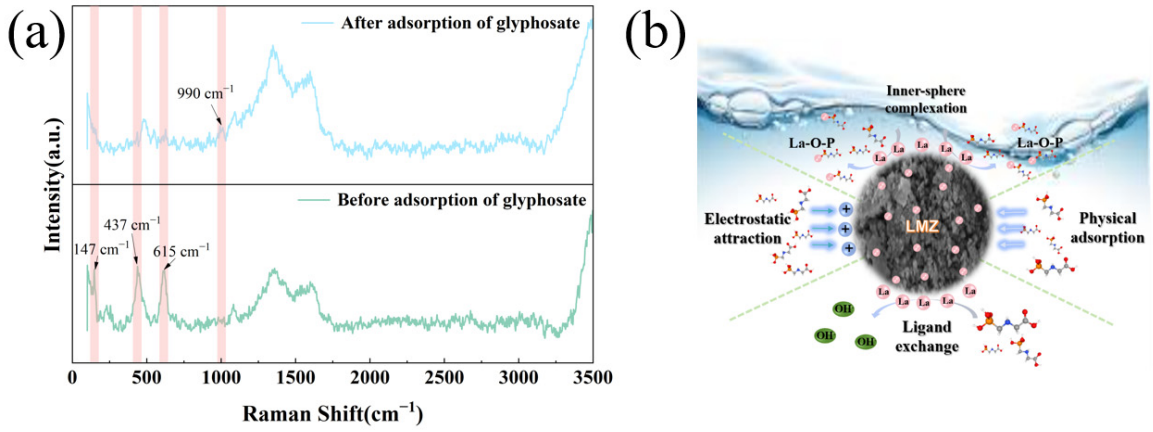

Figure 6. (**a**) Raman spectra of LMZ before or after glyphosate adsorption, (**b**) adsorption Mechanism of LMZ for glyphosate.

3.7. Dynamic Adsorption Experiments

The method of dynamic adsorption is usually used in actual wastewater treatment. Figure 6 shows the dynamic adsorption properties of glyphosate by LMZ at different flow rates. It was observed that the breakthrough curves all presented a typical "S" shape. At the initial stage, the values of C_t/C_0 were close to zero, as the active sites were still occupied; this value increased gradually until 100% breakthrough was reached. The time of saturation adsorption decreased with the increase of flow velocity. For example, at the flow rate of 2.5 mL/min, the saturation time of adsorption was 360 min, and when the flow rate rose to 5 mL/min and 7.5 mL/min, the saturation time was shortened to 240 min and 120 min, respectively.

To further understand the dynamic adsorption behaviors, the breakthrough curve data were fitted using the Yoon-Nelson model and the Bohart-Adams model (Equations (7) and (8)). In these equations, C_t

represents the concentration of glyphosate at time t (mg·L^{-1}), C_0 is the initial concentration of glyphosate (mg·L^{-1}), and t is the adsorption time (min). k_{YN} is the Yoon-Nelson rate constant (min^{-1}), and τ is the time required for 50% breakthrough (min). V denotes the linear velocity (cm·min^{-1}), k_{AB} is the Bohart-Adams rate constant (mL·mg^{-1}·min^{-1}), Z is the bed depth (cm), and N_0 is the saturation concentration of the fixed bed (mg·L^{-1}). The corresponding fitting parameters are presented in Table 1. The half penetration times predicted by Yoon-Nelson model for glyphosate decreased from 139.5 min at 2.5 mL/min to 32.7 min at 7.5 mL/min. This proves that the adsorption rate in the column is positively correlated with the flow rate [50].

Yoon-Nelson model

$$\frac{C_t}{C_0} = \frac{1}{1 + \exp\left(-k_{YN}(t - \tau)\right)} \tag{7}$$

Bohart-Adams model

$$\frac{C_t}{C_0} = \frac{1}{1 + \left(e^{\frac{k_{AB}N_0Z}{V}} - 1\right) \times e^{-k_{AB}C_0t}} \tag{8}$$

The adsorption capacity of the fixed bed at varying flow rates was calculated using the following equation (Equation (9)), with the results illustrated in Figure 7b. In this equation, q_t represents the adsorption capacity of the fixed bed at different effluent times; C_t is the effluent concentration of glyphosate at time t (mg·L^{-1}); the variable C_0 denotes the initial glyphosate concentration (mg·L^{-1}); the variable v denotes the flow rate (mL·min^{-1}); and the variable m denotes the mass of the adsorbent loaded (g). Clearly, the adsorption capacity decreased with increasing flow velocity. At the flow rate of 2.5 mL·min^{-1}, the adsorption capacity by La–Z was 116 mg·g^{-1}, and when the flow rate rose to 5 mL·min^{-1} and 7.5 mL·min^{-1}, the adsorption capacity dropped to 91 mg·g^{-1} and 84 mg·g^{-1}, respectively. These different adsorption behaviors were due to the different residence times of the solution in the column, which were insufficient at high flow rates. Thus, the glyphosate ions could not be effectively captured by LMZ, and the column was more easily penetrated, resulting in a reduction in adsorption capacity. In summary, this material demonstrates significant potential for practical water treatment applications. Regarding the final disposal of the spent adsorbent, high-temperature calcination can be employed to completely destroy the adsorbed organophosphorus structures. Subsequently, the remaining lanthanum-containing zeolite residue can be safely solidified and utilized as construction aggregates or road base materials, thereby effectively eliminating the risk of secondary pollution.

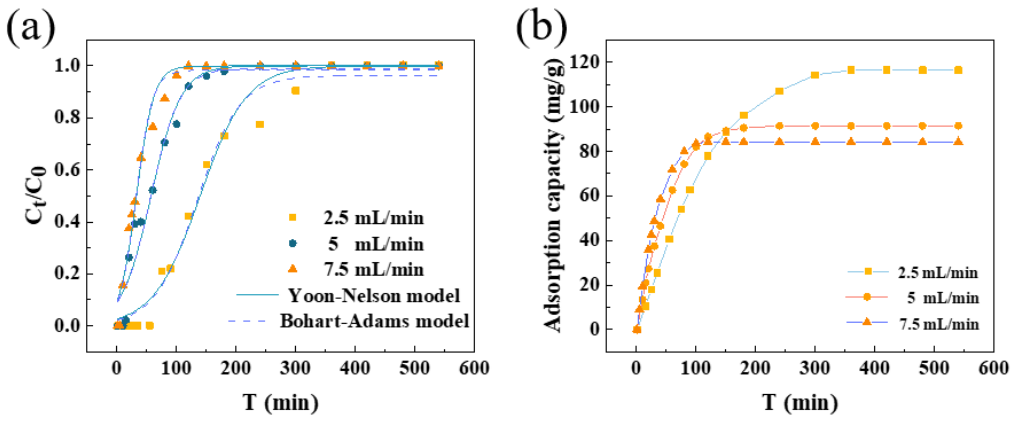

Figure 7. (**a**) Effect of flow rate on the breakthrough curve, (**b**) Dynamic adsorption kinetics of glyphosate on the fixed bed column.

$$q_t = \frac{v\int_0^t (C_0 - C_t)d_t}{m} \tag{9}$$

Table 1. Dynamic model fitting parameters.

Model	Bohart-Adams Model			Yoon-Nelson Model		
Flow Rate ($mL \cdot min^{-1}$)	K_{AB} $mL \cdot mg^{-1} \cdot min^{-1}$	N_0 $mg \cdot L^{-1}$	R^2	K_{YN} min^{-1}	τ min	R^2
2.5	8.4	0.031	0.981	0.026	139.5	0.979
5.0	12.3	0.017	0.969	0.040	57.3	0.968
7.5	21.6	0.011	0.977	0.068	32.7	0.976

4. Conclusions

In this paper, a highly efficient adsorbent of lanthanum modified zeolite was prepared, which demonstrated excellent adsorption performances for glyphosate. The LMZ could effectively capture glyphosate across a wide pH range, with a maximum adsorption capacity of 217.39 mg/g. The adsorption process follows the Langmuir model and the pseudo-second-order kinetic model, indicating that it is a monolayer adsorption involving a chemisorption mechanism. Indeed, the LMZ possessed excellent recyclability and anti-interference ability, with 85% of original adsorption capacity after five cycles. In the simulated wastewater experiment, the glyphosate removal efficiency can reach more than 90% at the dosage of 7.5 g/L. Moreover, the LMZ could maintain the adsorption performance even under dynamic adsorption conditions, and the adsorption rate was faster at high flow rate. The outstanding adsorption performance of LMZ for glyphosate was attributed to the multiple mechanisms, including ligand exchange, inner-complexation, and electrostatic attraction.

Supplementary Materials

The following supporting information can be found at: https://www.sciepublish.com/article/pii/1145, Figure S1: Adsorption of glyphosate onto LMZ at different temperatures; Figure S2: XRD patterns of zeolite and LMZ; Table S1: The fitting parameters of the isotherm models; Table S2: The fitting parameters of the kinetic models; Table S3: Chemical composition of LMZ determined by XRF analysis; Table S4: Comparison of the maximum adsorption capacities of various adsorbents for glyphosate. Table S5: Thermodynamic fitting parameters for glyphosate adsorption onto LMZ.

Acknowledgments

The work is funded by the Joint Funds of the National Natural Science Foundation of China (U24A2094), the Joint Funds for Innovation and Development of Natural Science Foundation of Hubei Province (2024AFD138), the National Natural Science Foundation of China (No. 52200201), the Natural Science Foundation of Hubei Province (No. 2022CFB698).

Author Contributions

Writing-original draft, Methodology, Investigation, X.Z. and J.L.; Datacuration, M.D.; Writing-review& editing, Formal analysis, Data curation, X.L.; Visualization, J.Y. (Jinming Yi) and S.L.; Formal analysis, J.Y. (Junxia Yu) and C.X.; Supervision, Y.Z. and R.C.; Resources, B.H. and J.C.; Project administration, S.Z.

Ethics Statement

Not applicable.

Informed Consent Statement

Not applicable.

Data Availability Statement

Data will be made available on request.

Funding

The work is funded by the Joint Funds of the National Natural Science Foundation of China (U24A2094), the Joint Funds for Innovation and Development of Natural Science Foundation of Hubei Province (2024AFD138), the National Natural Science Foundation of China (No. 52200201), the Natural Science Foundation of Hubei Province (No. 2022CFB698).

Declaration of Competing Interest

The authors declare that they have no known competing financial interests or personal relationships that could have appeared to influence the work reported in this paper.

References

1. Meng W, Li X, Yu J, Xiao C, Hou H, Chi R, et al. Ferrihydrite-loaded water hyacinth-derived biochar for efficient removal of glyphosate from aqueous solution. *Environ. Sci. Pollut. Res.* **2023**, *30*, 57410–57422. DOI:10.1007/s11356-023-26612-2
2. Matozzo V, Fabrello J, Marin MG. The Effects of Glyphosate and Its Commercial Formulations to Marine Invertebrates: A Review. *J. Mar. Sci. Eng.* **2020**, *8*, 399. DOI:10.3390/jmse8060399
3. Benbrook CM. Trends in glyphosate herbicide use in the United States and globally. *Environ. Sci. Eur.* **2016**, *28*, 3. DOI:10.1186/s12302-016-0070-0
4. Liu R, Xie Y, Cui K, Xie J, Zhang Y, Huang Y. Adsorption behavior and adsorption mechanism of glyphosate in water by amino-MIL-101(Fe). *J. Phys. Chem. Solids* **2022**, *161*, 110403. DOI:10.1016/j.jpcs.2021.110403
5. Botten N, Wood LJ, Werner JR. Glyphosate remains in forest plant tissues for a decade or more. *For. Ecol. Manag.* **2021**, *493*, 119259. DOI:10.1016/j.foreco.2021.119259
6. Viti ML, Alves PAT, Mendes KF, Pimpinato RF, Guimarães ACD, Tornisielo VL. Translocation and Root Exudation of Glyphosate by Urochloa brizantha and its Transport on Sugarcane and Citrus Seedlings. *Planta Daninha* **2019**, *37*, e019183334. DOI:10.1590/s0100-83582019370100030
7. Assalin MR, De Moraes SG, Queiroz SCN, Ferracini VL, Duran N. Studies on degradation of glyphosate by several oxidative chemical processes: Ozonation, photolysis and heterogeneous photocatalysis. *J. Environ. Sci. Health Part B* **2009**, *45*, 89–94. DOI:10.1080/03601230903404598
8. Koller VJ, Fürhacker M, Nersesyan A, Mišík M, Eisenbauer M, Knasmueller S. Cytotoxic and DNA-damaging properties of glyphosate and Roundup in human-derived buccal epithelial cells. *Arch. Toxicol.* **2012**, *86*, 805–813. DOI:10.1007/s00204-012-0804-8
9. Feng D, Soric A, Boutin O. Treatment technologies and degradation pathways of glyphosate: A critical review. *Sci. Total Environ.* **2020**, *742*, 140559. DOI:10.1016/j.scitotenv.2020.140559
10. Chen X, Yao XW, Diao Y, Liu H, Chen ML, Feng NJ, et al. Simultaneous removal of triadimefon and dinotefuran by a new biochar-based magnesium oxide composite in water: Performances and mechanism. *Sep. Purif. Technol.* **2024**, *336*, 126213. DOI:10.1016/j.seppur.2023.126213
11. Yao XW, Chen X, Chen ML, Feng NJ, Tong LY, Yi YQ, et al. Removal of pesticide acetamiprid using KOH activated biochar derived from crayfish shell: Behavior and mechanism. *Process Saf. Environ. Prot.* **2024**, *186*, 808–818. DOI:10.1016/j.psep.2024.04.076

12. Kang R, Yu J, Li X, Guo L, Xiao C, Chi R, et al. Efficient treatment of glyphosate mother liquor by a coagulation and adsorption combined process. *Colloids Surf. A Physicochem. Eng. Asp.* **2024**, *690*, 133811. DOI:10.1016/j.colsurfa.2024.133811
13. da Silva VEC, Tadayozzi YS, Putti FF, Santos FA, Forti JC. Degradation of commercial glyphosate-based herbicide via advanced oxidative processes in aqueous media and phytotoxicity evaluation using maize seeds. *Sci. Total Environ.* **2022**, *840*, 156656. DOI:10.1016/j.scitotenv.2022.156656
14. Chen Y, Chen WJ, Huang Y, Li J, Zhong J, Zhang W, et al. Insights into the microbial degradation and resistance mechanisms of glyphosate. *Environ. Res.* **2022**, *215*, 114153. DOI:10.1016/j.envres.2022.114153
15. Martins-Gomes C, Silva TL, Andreani T, Silva AM. Glyphosate *vs*. Glyphosate-Based Herbicides Exposure: A Review on Their Toxicity. *J. Xenobiot.* **2022**, *12*, 21–40. DOI:10.3390/jox12010003
16. He Q, Zhao H, Teng Z, Wang Y, Li M, Hoffmann MR. Phosphate removal and recovery by lanthanum-based adsorbents: A review for current advances. *Chemosphere* **2022**, *303*, 134987. DOI:10.1016/j.chemosphere.2022.134987
17. Wu Y, Li X, Yang Q, Wang D, Xu Q, Yao F, et al. Hydrated lanthanum oxide-modified diatomite as highly efficient adsorbent for low-concentration phosphate removal from secondary effluents. *J. Environ. Manag.* **2019**, *231*, 370–379. DOI:10.1016/j.jenvman.2018.10.059
18. Huang W, Zhu Y, Tang J, Yu X, Wang X, Li D, et al. Lanthanum-doped ordered mesoporous hollow silica spheres as novel adsorbents for efficient phosphate removal. *J. Mater. Chem. A* **2014**, *2*, 8839. DOI:10.1039/c4ta00326h
19. Jin H, Lin L, Meng X, Wang L, Huang Z, Liu M, et al. A novel lanthanum-modified copper tailings adsorbent for phosphate removal from water. *Chemosphere* **2021**, *281*, 130779. DOI:10.1016/j.chemosphere.2021.130779
20. Jia Z, Zeng W, Xu H, Li S, Peng Y. Adsorption removal and reuse of phosphate from wastewater using a novel adsorbent of lanthanum-modified platanus biochar. *Process Saf. Environ. Prot.* **2020**, *140*, 221–232. DOI:10.1016/j.psep.2020.05.017
21. Fotsop CG, Lieb A, Scheffler F. Highly efficient removal and separation of Sr^{2+}, Co^{2+}, In^{3+} and Ni^{2+} in single and mixed ion systems on low-cost Zeolite, and its stability analysis: DFT and experimental investigations. *Chem. Eng. J. Adv.* **2026**, *25*, 100986. DOI:10.1016/j.ceja.2025.100986
22. Sivalingam S, Sen S. Sono-assisted Adsorption of As(V) from Water by Rice-Husk-Ash-Derived Iron-Modified Mesoporous Zeolite Y: A Cradle-to-Cradle Solution to a Problematic Solid Waste Material. *Ind. Eng. Chem. Res.* **2019**, *58*, 14073–14087. DOI:10.1021/acs.iecr.9b01785
23. Chang Z, Yan Y, Bai L, Guo N, Xing Z, Lu C. Synthesis and Characterization of NaX Zeolite from Coal Gangue and Its Efficacy in Cd and Pb Remediation in Water and Soil. *ACS Omega* **2024**, *9*, 51237–51252. DOI:10.1021/acsomega.4c07708
24. Zhao M, Zhou X, Li J, Li F, Li X, Yu J, et al. Efficient removal of phosphate and fluoride from phosphogypsum leachate by lanthanum-modified zeolite: Synchronous adsorption behavior and mechanism. *J. Environ. Chem. Eng.* **2024**, *12*, 113294. DOI:10.1016/j.jece.2024.113294
25. Xie J, Wang Z, Fang D, Li C, Wu D. Green synthesis of a novel hybrid sorbent of zeolite/lanthanum hydroxide and its application in the removal and recovery of phosphate from water. *J. Colloid Interface Sci.* **2014**, *423*, 13–19. DOI:10.1016/j.jcis.2014.02.020
26. Li X, Zhang Z, Xie Q, Wu D. Effect of algae on phosphorus immobilization by lanthanum-modified zeolite. *Environ. Pollut.* **2021**, *276*, 116713. DOI:10.1016/j.envpol.2021.116713
27. Zavareh S, Farrokhzad Z, Darvishi F. Modification of zeolite 4A for use as an adsorbent for glyphosate and as an antibacterial agent for water. *Ecotoxicol. Environ. Saf.* **2018**, *155*, 1–8. DOI:10.1016/j.ecoenv.2018.02.043
28. Guo Y, Yu J, Li X, Guo L, Xiao C, Chi R, et al. Selective recovery of glyphosine from glyphosate mother liquor using a modified biosorbent: Competitive substitution adsorption. *Environ. Res.* **2022**, *215*, 114394. DOI:10.1016/j.envres.2022.114394
29. Shi W, Fu Y, Jiang W, Ye Y, Kang J, Liu D, et al. Enhanced phosphate removal by zeolite loaded with Mg–Al–La ternary (hydr)oxides from aqueous solutions: Performance and mechanism. *Chem. Eng. J.* **2019**, *357*, 33–44. DOI:10.1016/j.cej.2018.08.003
30. He Y, Lin H, Dong Y, Wang L. Preferable adsorption of phosphate using lanthanum-incorporated porous zeolite: Characteristics and mechanism. *Appl. Surf. Sci.* **2017**, *426*, 995–1004. DOI:10.1016/j.apsusc.2017.07.272
31. Koilraj P, Sasaki K. Selective removal of phosphate using La-porous carbon composites from aqueous solutions: Batch and column studies. *Chem. Eng. J.* **2017**, *317*, 1059–1068. DOI:10.1016/j.cej.2017.02.075
32. He Y, Lin H, Dong Y, Liu Q, Wang L. Simultaneous removal of ammonium and phosphate by alkaline-activated and lanthanum-impregnated zeolite. *Chemosphere* **2016**, *164*, 387–395. DOI:10.1016/j.chemosphere.2016.08.110

33. Lai KC, Hiew BYZ, Lee LY, Gan S, Thangalazhy-Gopakumar S, Chiu WS, et al. Ice-templated graphene oxide/chitosan aerogel as an effective adsorbent for sequestration of metanil yellow dye. *Bioresour. Technol.* **2019**, *274*, 134–144. DOI:10.1016/j.biortech.2018.11.048
34. Wu FC, Tseng RL, Juang RS. Initial behavior of intraparticle diffusion model used in the description of adsorption kinetics. *Chem. Eng. J.* **2009**, *153*, 1–8. DOI:10.1016/j.cej.2009.04.042
35. Qiu H, Liang C, Yu J, Zhang Q, Song M, Chen F. Preferable phosphate sequestration by nano-La(III) (hydr)oxides modified wheat straw with excellent properties in regeneration. *Chem. Eng. J.* **2017**, *315*, 345–354. DOI:10.1016/j.cej.2017.01.043
36. Acelas NY, Martin BD, López D, Jefferson B. Selective removal of phosphate from wastewater using hydrated metal oxides dispersed within anionic exchange media. *Chemosphere* **2015**, *119*, 1353–1360. DOI:10.1016/j.chemosphere.2014.02.024
37. Wang J, Wu L, Li J, Tang D, Zhang G. Simultaneous and efficient removal of fluoride and phosphate by Fe-La composite: Adsorption kinetics and mechanism. *J. Alloys Compd.* **2018**, *753*, 422–432. DOI:10.1016/j.jallcom.2018.04.177
38. Yang Y, Deng Q, Yan W, Jing C, Zhang Y. Comparative study of glyphosate removal on goethite and magnetite: Adsorption and photo-degradation. *Chem. Eng. J.* **2018**, *352*, 581–589. DOI:10.1016/j.cej.2018.07.058
39. Kovács N, Maász G, Galambos I, Gerencsér-Berta R, Mihály J, Tombácz E. Glyphosate/AMPA adsorption on magnetite under different conditions: The effect of pH and electrolytes. *J. Mol. Liq.* **2024**, *393*, 123674. DOI:10.1016/j.molliq.2023.123674
40. Waiman CV, Arroyave JM, Chen H, Tan W, Avena MJ, Zanini GP. The simultaneous presence of glyphosate and phosphate at the goethite surface as seen by XPS, ATR-FTIR and competitive adsorption isotherms. *Colloids Surf. A Physicochem. Eng. Asp.* **2016**, *498*, 121–127. DOI:10.1016/j.colsurfa.2016.03.049
41. Wang Y, Li H, Zhao Y, Qi M, Wang L, Feng J. Phosphate recovery from wastewater via vivianite crystallization using separable ferrous modified biochar beads. *Chem. Eng. J.* **2024**, *498*, 155453. DOI:10.1016/j.cej.2024.155453
42. Liu D, Li Y, Liu C, Zhou Y. Facile preparation of UiO-66@PPy nanostructures for rapid and efficient adsorption of fluoride: Adsorption characteristics and mechanisms. *Chemosphere* **2022**, *289*, 133164. DOI:10.1016/j.chemosphere.2021.133164
43. Su Y, Cui H, Li Q, Gao S, Shang JK. Strong adsorption of phosphate by amorphous zirconium oxide nanoparticles. *Water Res.* **2013**, *47*, 5018–5026. DOI:10.1016/j.watres.2013.05.044
44. Hena S, Patil KS, Leinecker N, Bhatelia T, Shah M. Effect of algal organic matter on adsorption of glyphosate using coconut shell-activated carbon. *Chem. Eng. J. Adv.* **2025**, *22*, 100754. DOI:10.1016/j.ceja.2025.100754
45. Xie X, Xie Y, Zuo K, Wu J, Fu S, Li W, et al. Nanosized lanthanum peroxide–loaded biochar composites for simple and effective glyphosate removal from wastewater: Behavior and mechanisms. *J. Clean. Prod.* **2024**, *447*, 141451. DOI:10.1016/j.jclepro.2024.141451
46. Yan W, Jing C. Molecular Insights into Glyphosate Adsorption to Goethite Gained from ATR-FTIR, Two-Dimensional Correlation Spectroscopy, and DFT Study. *Environ. Sci. Technol.* **2018**, *52*, 1946–1953. DOI:10.1021/acs.est.7b05643
47. Ruano G, Pedano ML, Albornoz M, Fuhr JD, Martiarena ML, Zampieri G. Deprotonation of the amine group of Glyphosate studied by XPS and DFT. *Appl. Surf. Sci.* **2021**, *567*, 150753. DOI:10.1016/j.apsusc.2021.150753
48. Khoury GA, Gehris TC, Tribe L, Torres Sánchez RM, dos Santos Afonso M. Glyphosate adsorption on montmorillonite: An experimental and theoretical study of surface complexes. *Appl. Clay Sci.* **2010**, *50*, 167–175. DOI:10.1016/j.clay.2010.07.018
49. Zhang L, Liu Y, Wang Y, Li X, Wang Y. Investigation of phosphate removal mechanisms by a lanthanum hydroxide adsorbent using p-XRD, FTIR and XPS. *Appl. Surf. Sci.* **2021**, *557*, 149838. DOI:10.1016/j.apsusc.2021.149838
50. Liu Y, Yu JX, Guo L, Song G, Li X, Xiao C, et al. Insight into a novel circulation system combined with coordination leaching and biosorption for Cu(II) efficient recycling from electroplating sludge. *Sep. Purif. Technol.* **2024**, *334*, 125948. DOI:10.1016/j.seppur.2023.125948